Phonon-Assisted Magnetic Mott-Insulating State in the Charge Density Wave Phase of Single-Layer 1T-$NbSe_2$

Matteo Calandra*
Sorbonne Université, CNRS, Institut des Nanosciences de Paris, UMR7588, F-75252 Paris, France

(Received 13 March 2018; published 10 July 2018)

We study the structural, electronic, and vibrational properties of single-layer 1T-$NbSe_2$ from first principles. Within the generalized gradient approximation, the 1T polytype is highly unstable with respect to the 2H. The density functional theory with the Hubbard U method improves the stability of the 1T phase, explaining its detection in experiments. A charge density wave occurs with a $\sqrt{13}\times\sqrt{13}R30°$ periodicity, in agreement with STM data. At $U=0$, the David-star reconstruction displays a flatband below the Fermi level with a marked $d_{z^2-r^2}$ orbital character of the central Nb. The Hubbard interaction induces a magnetic Mott-insulating state. Magnetism distorts the lattice around the central Nb atom in the star, reduces the hybridization between the central Nb $d_{z^2-r^2}$ orbital and the neighboring Se p states, and lifts in energy the empty $d_{z^2-r^2}$ flatband becoming nonbonding. This cooperative Jahn-Teller and correlation effect amplifies the Mott gap. Our results are relevant for the broad class of correlated insulator in the presence of a strong Jahn-Teller effect.

DOI: 10.1103/PhysRevLett.121.026401

The 2H polytypes of transition metal dichalcogenides, like 2H-$NbSe_2$, 2H-TaS_2, or 2H-$TaSe_2$, are ideal materials to study the interplay of superconductivity and charge density wave (CDW) [1], as the electron-electron interaction has a minor role and metallicity survives in the CDW state. 1T polytypes, such as 1T-$TiSe_2$, 1T-TaS_2, or 1T-$TaSe_2$, are substantially different and more critical, as in the CDW ground state the electron-electron interaction is supposed to substantially affect the electronic structure [2–4] and lead to Mott [5], Slater, or magnetic-insulating states and even to spin liquids [6]. While 1T-$TaSe_2$ is metallic at low temperature, the CDW state of 1T-$TiSe_2$ seems to have a very small electronic gap (0.1 eV). The nature of the low-temperature state of 1T-TaS_2 is still very controversial, as it has been proposed to be a Mott insulator [5], an Anderson disordered insulator [4], or more recently, a metal [7].

The electronic structure of the high-T phase of 1T polytypes in the absence of a CDW (hereby labeled high-symmetry structure) can be understood, to some extent, by neglecting interlayer coupling and invoking the crystal-field symmetry around the transition metal (TM) [8,9]. The chalcogene atoms form a slightly distorted octahedron around the TM, as shown in Fig. 1(a). In the case of an undistorted octahedron, the atomic d levels are split into triply degenerate t_{2g} orbitals ($d_{x^2-y^2}$, $d_{z^2-r^2}$, d_{xy}) and doubly degenerate e_g orbitals (d_{xy}, d_{xz}) at higher energy. The distortion of the octahedron breaks the degeneracy of the t_{2g} manifold and lowers the energy of the $d_{z^2-r^2}$ orbital. For the case of Ta or Nb, the nominal d^1 valence leads to an half-filled $d_{z^2-r^2}$ state at zone center [see Fig. 1(b)], with the exact position of the Fermi level depending on the hybridization between the chalcogene and the TM orbitals.

In the case of a $\sqrt{13}\times\sqrt{13}R30°$ CDW with the formation of a so-called David-star clustering, each one of the 13 $d_{z^2-r^2}$ states involved in the star carries one electron, leading to a formally half-filled HOMO molecular state. The narrowness of the HOMO state, related to the weaker interstar interaction, is prone to electronic instabilities. Indeed it has been suggested [5] that bulk 1T-TaS_2 is a Mott insulator. The experimental validation of this scenario in 1T-TaS_2 has proven to be very controversial mainly due to the experimental incertitude in the determination of the interlayer stacking[10–13] and the consequent orbital ordering affecting hopping along the c axis. Moreover, the occurrence of Jahn-Teller distortion within the $\sqrt{13}\times\sqrt{13}R30°$ pattern emerging from the stabilization of a spin-1/2 magnetic state on each star has never been discussed. Finally, recent angle-resolved photoemission spectroscopy (ARPES) experiments [7] display a metallic band dispersion along k_z, meaning that the ground state of 1T-TaS_2 is still very controversial.

The validity of the Mott scenario could be addressed by synthesizing 1T-TaS_2 single layers; however, this attempt has been, for the moment, unsuccessful as (i) single-layer TaS_2 grown epitaxially on Au(111) assumes the 2H polytype [14] and (ii) preliminary results on exfoliated suspended samples seem to show that the 1T-TaS_2 single layer undergoes a different kind of CDW order [15]. Although some supported samples show Raman spectra

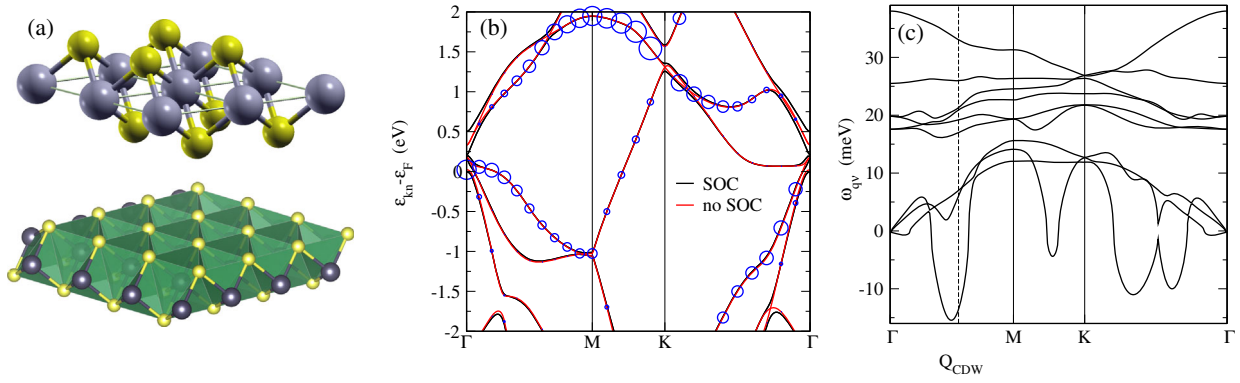

FIG. 1. (a) Crystal structure of an undistorted $1T$-$NbSe_2$ single layer (Nb atoms in gray, Se atoms in yellow). In the bottom image, the octahedral coordination around the Nb atom is shown. Electronic structure (b) and phonon dispersion (c) of single-layer $1T$-$NbSe_2$ in the high-symmetry phase. In (b) SOC (no SOC) means with (without) inclusion of spin-orbit coupling. In the nonrelativistic case, the size of the blue dots is proportional to the $3d_{z^2-r^2}$ orbital component (at $\mathbf{\Gamma}$, the larger dot corresponds to a 53% $d_{z^2-r^2}$ component).

consistent with a $\sqrt{13}\times\sqrt{13}R30°$ CDW [16], nothing is known on the nature of their electronic structure.

A way out of this impasse is to consider the $1T$-$NbSe_2$ single layer. Although in bulk form and in most exfoliated samples $NbSe_2$ assumes the $2H$ polytype, it has been recently shown that a single layer of $1T$ polytype can be grown epitaxially on bilayer graphene [17], keeping the substrate at temperatures larger than 500 K. Scanning tunneling spectroscopy (STS) shows the occurrence of a $\sqrt{13}\times\sqrt{13}R30°$ CDW. ARPES and STS measurements in the CDW phase seem to show the occurrence of an ≈0.3–0.4 eV gap at zone center. No measurements of the band structure in other regions of the Brillouin zone are available at the moment. Not surprisingly, the ARPES data in the CDW phase are in stark disagreement with electronic structure calculations in the high-symmetry $1T$-$NbSe_2$ phase [17]. Finally, and most interesting, Bischoff *et al.* [18] recently showed that it is possible to transform the surface of exfoliated $2H$-$NbSe_2$ samples into a $1T$-$NbSe_2$ phase by applying a STM bias pulse of 4 V for 100 ms. The $1T$-$NbSe_2$ phase in the top layer is then (meta) stable at 77 K and displays the occurrence of the characteristic $\sqrt{13}\times\sqrt{13}R30°$ reconstruction.

In this Letter, by using electronic structure calculations [19,20], we show that single-layer $1T$-$NbSe_2$ undergoes a CDW instability with a $\sqrt{13}\times\sqrt{13}R30°$ reconstruction, in agreement with experiments. A cooperative correlation and Jahn-Teller effect stabilizes a spin-1/2 magnetic Mott-insulating state in reduced dimension.

We first consider the high-symmetry $1T$-$NbSe_2$ structure shown in Fig. 1. We use the in-plane experimental lattice parameter ($a_{\mathrm{Expt}} = 3.44$ Å) and minimize the internal coordinates. More technical details are given in the Supplemental Material [21]. The calculated electronic structure shown in Fig. 1(b) is similar to that of the undistorted $1T$-TaS_2 monolayer [4]; however, the hybridization between chalcogene and TM d orbitals is much stronger in this case so that the bottom of the $d_{z^2-r^2}$ band is substantially lower in energy and there is no gap between Nb d and Se p states. Finally, as the $1T$ structure breaks inversion symmetry, we carry out a fully relativistic electronic structure calculation, but we found the spin-orbit coupling to be negligible for the undistorted phase, as shown in Fig. 1(b). For this reason, we neglect relativistic effects in the rest of the Letter.

We calculate the vibrational properties of the high-symmetry $1T$-$NbSe_2$ phase and, not surprisingly, we find strongly unstable phonon modes [Fig. 1(c)] with the largest instability very close to the ordering vector $\mathbf{Q}_{\mathrm{CDW}} = 2\pi/\sqrt{13}a(1,0)$, which is the nearest vector along

TABLE I. Energetics of single-layer $NbSe_2$ polytypes with respect to the high-symmetry $2H$-$NbSe_2$ polytype, $\Delta E = E - E(2\mathrm{H})$, as a function of U. The labels $\Delta E(U=0,\mathrm{Expt})$, $\Delta E(U=2.95,\mathrm{Expt})$ mean that the internal coordinates have been optimized at fixed volume using the experimental lattice parameters and the GGA + U functional with $U=0$ and $U=2.95$ eV, respectively. The labels $\Delta E(U=0,\mathrm{Opt})$ and $\Delta E(U=2.95,\mathrm{Opt})$ refer to complete structural optimization of internal coordinates and volume using the GGA + U approximation with $U=0$ and $U=2.95$ eV, respectively. The energy units are mRy per Nb atom and U is expressed in eV. The values of the experimental (Expt.) and optimized (Opt.) cell parameter are shown (in angstrom). We use as the experimental lattice parameter the in plane one of the bulk, namely, $a_{\mathrm{Expt}} = 3.44$ Å.

Structure	$\Delta E(U=0,\mathrm{Expt})$	$\Delta E(U=2.95,\mathrm{Expt})$	$\Delta E(U=0,\mathrm{Opt})$	$\Delta E(U=2.95,\mathrm{Opt})$	$a(U=0)$	$a(U=2.95)$
$2H$ high symmetry	0.0	0.0	0.0	0.0	3.473	3.451
$1T$ high symmetry	+7.2	+4.2	+7.3	+4.4	3.482	3.464
$1T$ CDW	+3.0	−1.1	+2.9	−1.6	12.575	12.523

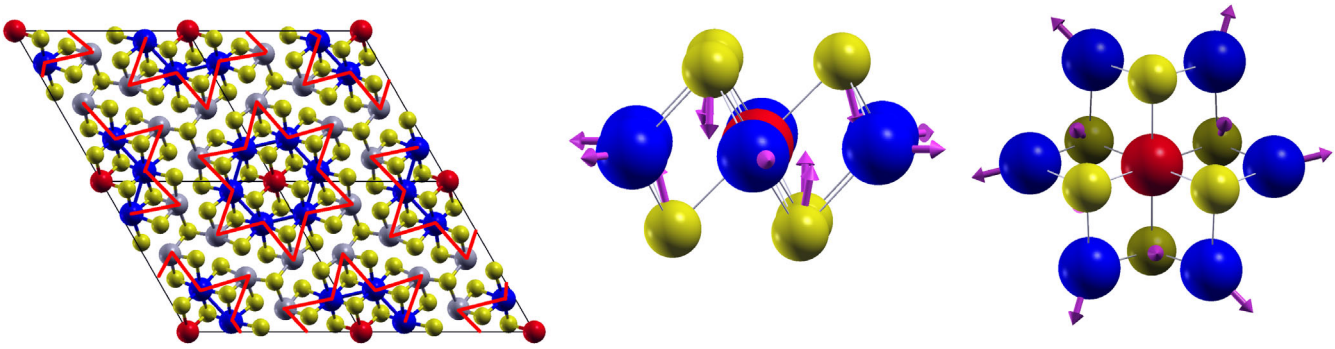

FIG. 2. (Left) Optimized crystal structure for the low-temperature phase of 1T-$NbSe_2$. There are three inequivalent Nb sites: central Nb (red), hexagonal site belonging to the $\sqrt{7} \times \sqrt{7}$ cluster (blue), and peripheral Nb sites (gray). The Se atoms are shown in yellow. The red line is a guide to the eye to recognize the $\sqrt{13} \times \sqrt{13}$ cluster (David star). The inclusion of the Hubbard term leads to a ferromagnetic state with an important local distortion around the central Nb atom in the star. However, the difference between the ferromagnetic and nonmagnetic structures are not visible on this scale. The magnetic state has a total magnetization of $+1\mu_B$. The magnetic moments on Nb atoms are $0.58\mu_B$ central (red) Nb, 0.0417 (blue) Nb, -0.0256 peripheral (gray) Nb. The moduli of the magnetic moments on Se atoms are smaller than $0.08\mu_b$. (Center and left) Magnetic-induced distortion (side and top views) in the central $\sqrt{7} \times \sqrt{7}$ cluster. The central atom is unshifted. The six blue Nb atoms interacting ferromagnetically with the central one moves apart in plane. The out-of-plane Se approaches the Nb basal plane. In the top view (right) the bottom Se atoms are shown in a darker yellow color.

ΓM compatible with a $\sqrt{13} \times \sqrt{13}$ distortion (see Ref. [22], Fig. 1, right). We then consider a $\sqrt{13} \times \sqrt{13}R30°$ supercell and perform structural optimization assuming a nonmagnetic state. We obtain the David-star structure depicted in Fig. 2 and reported in the Supplemental Material [21]. The structure has three inequivalent Nb sites: central (red), hexagonal site belonging to the $\sqrt{7} \times \sqrt{7}$ cluster (blue), and peripheral (gray). The energy gain of the CDW structure with respect to the nonmagnetic high-symmetry 1T structure is very large (4.2 mRy/Nb); however, the CDW structure is still substantially disfavored from the 2H high-symmetry structure (see Table I). Thus, on the basis of nonmagnetic calculations, it would be very difficult to detect any 1T-$NbSe_2$ polytype.

Despite the large number of atoms in the cell, the electronic structure at the Fermi level is fairly simple. The top of the valence band is at zone center and is composed mostly of Se states originating from all the chalcogenes in the star. At the Fermi level, there is a very flat band having a marked $d_{z^2-r^2}$ character from the central Nb atom (red dots in Fig. 3). The band has several avoided crossings due to the reduced symmetry of the CDW state. As it will be soon clear, tracking the central-atom $d_{z^2-r^2}$ orbital component allows us to detect the upper and lower Hubbard bands.

The narrowness of the band suggests the possible occurrence of electronic instabilities. Then, in an effort to stabilize a magnetic state, we perform a spin-polarized generalized gradient approximation (GGA) on top of the GGA [23] nonmagnetic geometry. However, we always converge to a nonmagnetic state. We then consider the GGA + U approximation as implemented in Ref. [24]. We calculate the Hubbard U self-consistently [25] and obtain $U = 2.95$ eV, slightly larger than what has been obtained in 1T-TaS_2 [4]. We then perform magnetic calculations within this approximation. We now find that the ground state of single-layer 1T-$NbSe_2$ in the $\sqrt{13} \times \sqrt{13}R30°$ phase is ferromagnetic with a total spin magnetization of $1\mu_B$ per cell and an absolute magnetization (sum of the modulus of the magnetic moments on all atoms in the cell) of $2.2\mu_B$.

Before proceeding further, it is very instructive to consider the effect of the Hubbard correction and of the stabilization of a magnetic state on the energetics of the different polytypes of single-layer $NbSe_2$. Complete structural optimization within the GGA + U method leads to cell parameters in excellent agreement with experimental data, even for what concerns the 2H nonmagnetic high-symmetry structure (see Table I), with essentially no change in its electronic structure (see [21]). The GGA + U corrects the GGA underbinding error. The energy differences between the nonmagnetic 1T and 2H high-symmetry structures is still large, but substantially reduced, suggesting that the high-symmetry 1T phase cannot be easily stabilized. The only effect of the GGA + U approximation on the electronic structure of the high-symmetry phase of single-layer 1T-$NbSe_2$ is to unmix Se p and Nb d states at the Fermi level at zone center (see [21]). Most important, the total energy of the magnetic $\sqrt{13} \times \sqrt{13}R30°$ structure has a 1.6 mRy energy gain with respect to the 2H-$NbSe_2$ high-symmetry structure. The 1T-$NbSe_2$ CDW phase is comparable in energy with the high-symmetry structure. Thermal or kinetic effects stabilize then one or the other at 500 K.

In order to compare different approximations for the exchange correlation functional on the electronic structure, we stick to the experimental cell parameter, as cell

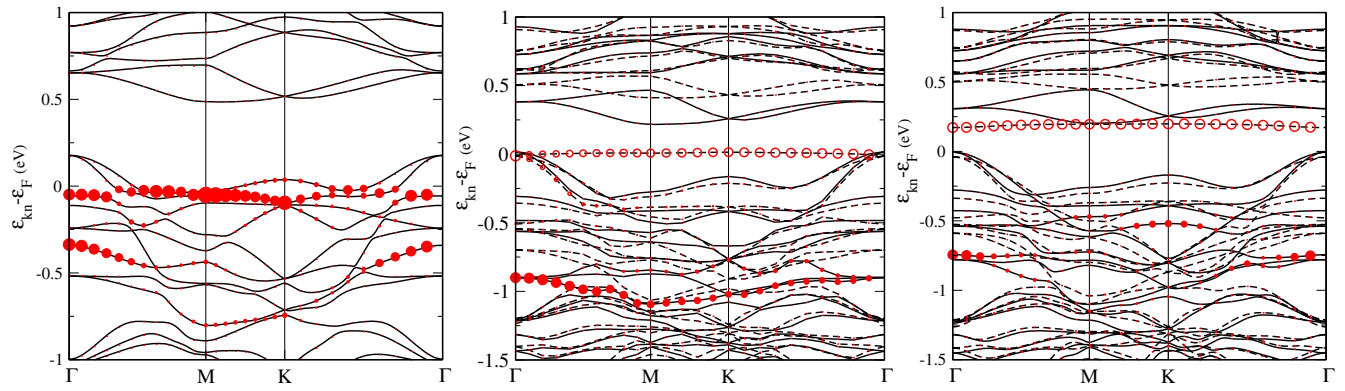

FIG. 3. (Left) Electronic structure in the charge density wave phase of $1T$-$NbSe_2$ within the nonmagnetic GGA. The size of the red dots is proportional to the Nb central-atom $d_{z^2-r^2}$ orbital character (the red dot at zone center and -0.05 eV corresponds to 15% orbital character). (Center) Same as the left but in the GGA + U approximation on top of the nonmagnetic geometry. Continuous (dashed) lines are majority (minority) spin bands. The size of the full (open) dots is proportional to the Nb central-atom $d_{z^2-r^2}$ up spin (down spin) orbital character. (Right) As in the center, but on top of the GGA + U geometry. The Hubbard-induced distortion raises in energy the minority spin band and increases the Mott gap.

relaxation is anyway marginal. We disentangle the magnitude of the Hubbard term from the magnetic-induced structural distortion by first calculating the electronic structure within the GGA + U approximation on top of the GGA geometry. A ferromagnetic state is stabilized even in this case with the opening of an Hubbard gap between the majority and minority bands having dominant $d_{z^2-r^2}$ character on the central Nb atom, as shown in Fig. 3 (see filled and open red dots in the center panel). However, the electronic structure is still metallic due to the residual hybridization between the $d_{z^2-r^2}$ central Nb and the nearest neighbors Se atoms.

Structural optimization of internal coordinates within the GGA + U approximation in the magnetic state leads to a substantial distortion of the $\sqrt{7}\times\sqrt{7}$ cluster around the central Nb (i.e., the six Nb atoms in blue in Fig. 2, left). If the GGA + U approximation with $U = 2.95$ eV is performed at clamped nuclei; i.e., it is carried out on the CDW structure obtained at $U = 0$ eV, the loss in total energy with respect to the fully optimized structure at $U =$ 2.95 eV is ≈0.8 mRy/Nb atom, corresponding to ≈30% of the total energy gain by the CDW distortion at $U = 0$ eV (see Table I).

The distortion leaves unshifted the central Nb atom, while the six nearest Nb atoms move in plane and apart from the central one and the out-of-plane Se atoms fill the empty space, reducing the distance with the Nb plane, as shown in Fig. 2 (center and right). The hybridization between the central Nb $d_{z^2-r^2}$ orbital and the nearest Se p states is reduced and the band degeneracy is removed by opening a gap in the spectrum, as in a molecular Jahn-Teller effect. The minority band with the largest Nb $d_{z^2-r^2}$ orbital component becomes nonbonding (see Fig. 3, right). The shift of the other atoms not belonging to the $\sqrt{7}\times\sqrt{7}$ cluster is minor, so that overall the David-star CDW is preserved. More quantitatively, using the experimental lattice parameter, the distance between the central Nb atom in the star and its neighboring Nb is ≈3.157 Å at $U = 0$ eV and ≈3.226 Å at $U = 2.95$ eV. Similarly, the distance between Se atoms of the $\sqrt{7}\times\sqrt{7}$ cluster from the Nb plane is decreased from ≈1.838 Å at $U = 0$ eV to 1.788 Å at $U = 2.95$ eV.

Thus, the insulating state in $1T$-$NbSe_2$ is not simply reached via a standard Mott mechanism, but a cooperative lattice and magnetic effect increases the Mott gap and amplifies the effect of the Hubbard interaction. Within GGA + U, single-layer $1T$-$NbSe_2$ is then a phonon-assisted spin-1/2 ferromagnetic Mott insulator displaying a $\sqrt{13}\times\sqrt{13}R30°$ David-star CDW.

It is worth mentioning that our calculated gap is approximately 0.18 eV smaller than the one detected in STM (0.3–0.4 eV) and ARPES in Ref. [17]. The gap does not seem to increase anymore with U, as for $U > 3.1$ eV, the flatband becomes higher in energy than the next two empty bands [21,26]. Recently, it was suggested [27] that the gap underestimation could be due to the lack of nonlocal exchange in the calculation. Besides this, other effects could also affect the gap size, like the presence of a graphene substrate leading to a non-negligible charge transfer or band bending occurring in STM. Nevertheless, it is important to underline that the valence band electronic structure is in good agreement with experimental data despite the large temperature broadening occurring in experiments [21].

In this Letter, by using first principles calculations, we have shown that single-layer $1T$-$NbSe_2$ undergoes a CDW instability with a $\sqrt{13}\times\sqrt{13}R30°$ reconstruction. However, the GGA leads to a substantially unstable $1T$-$NbSe_2$ structure with respect to the $2H$ polytypes. The GGA + U approximation improves the stability of all $1T$ polytypes, explaining the detection of $1T$-$NbSe_2$ in experiments. Moreover, it stabilizes a ferromagnetic state

with a spin magnetization of $1\mu_B$. Ferromagnetism occurs in the context of a flat d band, as in the ferromagnetic cuprate $LaBaCuO_5$ [28,29]. However, while in the latter the flatband is isolated and even the local spin density approximation stabilizes a sizable gapped ferromagnetic state, in $1T$-$NbSe_2$ the situation is more complicated by the non-negligible hybridization with Se states at zone center, and the framework is more that of a multiband Hubbard model. If the lattice is kept frozen at the nonmagnetic crystal structure, then hybridization hinders the opening of a Mott gap and favors a metallic state (or a state with a negligible gap). Thus, even if to some extent the long-standing proposal of Ref. [5], based on a purely electronic mechanism, partly applies to $1T$-$NbSe_2$, this is also not the complete explanation, as the opening of the gap occurs via a cooperative electronic and lattice (Jahn-Teller) effect, resulting from ferromagnetism and the subsequent Nb —Nb bond softening around the central Nb atom in the star. Even if for small values of $U < 3.1$ eV the size of the gap depends on the value of the Hubbard U parameter (which in our Letter is calculated from first principles self-consistently [25]), the distortion amplifies anyway the effect of the Hubbard term by reducing the hybridization (the larger U, the larger the local distortion).

We believe that the cooperative enhancement of the Mott gap due to electronic and lattice degrees of freedom is relevant far beyond the family of $1T$ dichalcogenides, but it is a genuine feature of correlated insulators in the presence of strong Jahn-Teller distortion. A similar mechanism was suggested to be relevant in manganites and manganese oxides [30] or in the fullerides like K_4C_{60} [31]. $1T$-$NbSe_2$ is an ideal playground to study Mott Jahn-Teller insulators in reduced dimension.

We acknowledge IDRIS, CINES, TGCC, and PRACE for high-performance computing resources, support from the European Union Horizon 2020 Research and Innovation Programme under Grant No. 696656-GrapheneCore1 and from Agence Nationale de la Recherche under the reference No. ANR-13-IS10-0003-01. We acknowledge M. Casula for useful discussions.

*matteo.calandra@upmc.fr

[1] J. A. Salvo, F. J. Di, and Mahajan, Adv. Phys. **24**, 117 (1975).
[2] K. Rossnagel, J. Phys. Condens. Matter **23**, 213001 (2011).
[3] R. Bianco, M. Calandra, and F. Mauri, Phys. Rev. B **92**, 094107 (2015).
[4] P. Darancet, A. J. Millis, and C. A. Marianetti, Phys. Rev. B **90**, 045134 (2014).
[5] P. Fazekas and E. Tosatti, Physica (Amsterdam) **99B**, 183 (1980); Philos. Mag. B **39**, 229 (1979).
[6] M. Klanjsek, A. Zorko, R. Zitko, J. Mravlje, Z. Jaglicic, P. K. Biswas, P. Prelovsek, D. Mihailovic, and D. Arcon, Nat. Phys. **13**, 1130 (2017).
[7] A. S. Ngankeu, S. K. Mahatha, K. Guilloy, M. Bianchi, C. E. Sanders, K. Hanff, K. Rossnagel, J. A. Miwa, C. B. Nielsen, M. Bremholm, and P. Hofmann, Phys. Rev B **96**, 195147 (2017).
[8] M.-H. Whangbo and E. Canadell, J. Am. Chem. Soc. **114**, 9587 (1992).
[9] L. F. Mattheiss, Phys. Rev. B **8**, 3719 (1973).
[10] A. Spijkerman, J. L. de Boer, A. Meetsma, G. A. Wiegers, and S. van Smaalen, Phys. Rev. B **56**, 13757 (1997).
[11] S. Tanda, T. Sambongi, T. Tani, and S. Tanaka, J. Phys. Soc. Jpn. **53**, 476 (1984).
[12] K. Nakanishi and H. Shiba, J. Phys. Soc. Jpn. **53**, 1103 (1984).
[13] L. Perfetti, T. A. Gloor, F. Mila, H. Berger, and M. Grioni, Phys. Rev. B **71**, 153101 (2005).
[14] C. E. Sanders, M. Dendzik, A. S. Ngankeu, A. Eich, A. Bruix, M. Bianchi, J. A. Miwa, B. Hammer, A. A. Khajetoorians, and P. Hofmann, Phys. Rev. B **94**, 081404 (2016).
[15] D. Sakabe, Z. Liu, K. Suenaga, K. Nakatsugawa, and S. Tanda, npj Quantum Mater. **2**, 22 (2017).
[16] O. R. Albertini, R. Zhao, R. L. McCann, S. Feng, M. Terrones, J. K. Freericks, J. A. Robinson, and A. Y. Liu, Phys. Rev. B **93**, 214109 (2016).
[17] Y. Nakata, K. Sugawara, R. Shimizu, Y. Okada, P. Han, T. Hitosugi, K. Ueno, T. Sato, and T. Takahashi, NPG Asia Mater. **8**, e321 (2016).
[18] F. Bischoff, W. Auwärter, J. V. Barth, A. Schiffrin, M. Fuhrer, and B. Weber, Chem. Mater. **29**, 9907 (2017).
[19] P. Giannozzi *et al.*, J. Phys. Condens. Matter **21**, 395502 (2009).
[20] P Giannozzi *et al.*, J. Phys. Condens. Matter **29**, 465901 (2017).
[21] See Supplemental Material at http://link.aps.org/supplemental/10.1103/PhysRevLett.121.026401 for technical details, structural parameters, electronic structure of $NbSe_2$ polytypes in the high-T phase, projected density of states plots, and comparison with ARPES data.
[22] Y. Ge and A. Y. Liu, Phys. Rev. B **82**, 155133 (2010).
[23] J. P. Perdew, K. Burke, and M. Ernzerhof, Phys. Rev. Lett. **77**, 3865 (1996).
[24] M. Cococcioni and S. de Gironcoli, Phys. Rev. B **71**, 035105 (2005).
[25] H. J. Kulik, M. Cococcioni, D. A. Scherlis, and N. Marzari, Phys. Rev. Lett. **97**, 103001 (2006).
[26] D. Pasquier and O. V. Yazyev, Phys. Rev. B **98**, 045114 (2018).
[27] E. Kamil *et al.*, arXiv:1804.03898.
[28] V. Eyert, K.-H. Höck, and P. S. Riseborough, Europhys. Lett. **31**, 385 (1995).
[29] W. Ku, H. Rosner, W. E. Pickett, and R. T. Scalettar, Phys. Rev. Lett. **89**, 167204 (2002).
[30] Y. Motome and M. Imada, J. Phys. Soc. Jpn. **68**, 16 (1999).
[31] M. Fabrizio and E. Tosatti, Phys. Rev. B **55**, 13465 (1997).